Flash Photolytic Studies of Carbon Monoxide Binding to the Ferrous Chains of [Mn(II),Fe(II)] Hybrid Hemoglobins: Kinetic Mechanism for the Early Stages of Hemoglobin Ligation†

Neil V. Blough,‡ Haya Zemel, and Brian M. Hoffman*

ABSTRACT: Flash photolysis is employed to investigate the kinetics of CO recombination to the ferrous chains of [Mn(II),Fe(II)] hemoglobin (Hb) hybrids. At low pH (6.6), Hb remains predominantly in the T quaternary state for the first two CO ligation steps, when binding to either the α chains or β chains. At elevated pH, CO binding to the α chains produces a larger degree of T to R conversion than binding to the β chains, in support of earlier equilibrium measurements. This study provides the full pH dependence of the CO binding rate constants for both α- and β-Fe chains within the T state and at elevated values of pH gives the R-state rate constants for the monoliganded analogues. The data can be analyzed within the context of a two-state model for Hb cooperativity, but they give clear evidence for slow quaternary structure interconversion at the monoliganded level.

Metal substitution, in the form of the mixed-metal [Mn(II),Fe(II)][1] hybrid hemoglobins, provides a particularly effective means with which to study the early stages of CO binding to Hb. In these hybrids, two chains of a single type, either α or β, are substituted with manganese(II) protoporphyrin IX, which does not bind CO. Equilibrium (Blough & Hoffman, 1982, 1984) and kinetic measurements (Blough et al., 1980) of CO binding and single-crystal X-ray diffraction studies[2] have shown that the [Mn(II),Fe(II)]hybrids are functional Hb analogues. They adopt the T state in the absence of ligands, and thus CO binding by the ferrous subunits represents those ligation processes in which the first ligands bind only to a single chain type, α or β.

To investigate the dynamics of these early Hb ligation steps, we have measured the kinetics of CO recombination subsequent to flash photolysis of the [Mn(II),Fe(II)(CO)] hybrids. These experiments show that at low pH, Hb remains predominantly in the T quaternary state when two CO have bound either to the α or to the β chains. This is consistent with equilibrium measurements (Blough & Hoffman, 1982, 1984) and X-ray diffraction results[2] and permits direct determination of rate constants for CO binding to individual chains within the T state (Blough et al., 1980). At elevated pH, equilibrium and kinetic measurements both indicate that significant T $\rightarrow$ R conversion occurs after two binding steps and that the degree of T $\rightarrow$ R conversion is greater for ligand binding to the α chains than to the β chains. However, the present results, in addition to those from studies of valency hybrids (Ogawa & Shulman, 1971; Cassoly et al., 1971; Ogawa & Shulman, 1972; Cassoly & Gibson, 1972; Rollema & deBruin, 1978), give clear evidence for slow quaternary structure interconversion at the mono- and diliganded levels of Hb ligation. This conclusion supports that of Sawicki & Gibson (1976, 1977) in that Hb kinetics cannot be understood fully within a two-state model involving rapid R $\rightleftarrows$ T equilibration (Hopfield et al., 1971).

Experimental Procedures

The [Mn(II),Fe(II)] hybrids were prepared and purified as previously described (Blough & Hoffman, 1984). Buffers at pH 6.6 contained 50 mM Bis-Tris-HCl, while buffers at pH 7.6, 8.0, and 9.0 were prepared with 50 mM Tris-HCl. Dithionite and methylene blue solutions were prepared as previously described; samples of the [Mn(II),Fe(II)(CO)] hybrids were prepared anaerobically within tonometers having 1-cm optical cells, as previously described (Blough & Hoffman, 1984). The heme concentrations in samples prepared in this manner varied between 3 and 8 μM. CO was introduced to the sample by flushing with 1 atm of CO or 5% CO in N_2 (Matheson, primary standard). Alternatively, intermediate CO concentrations were obtained by adding appropriate volumes of 100% CO to the tonometer. Samples with low concentrations of heme (0.1–0.5 μM) were prepared in 5-cm optical cells having two ports that were stoppered with silicone rubber septums (W-10, Applied Science Labs.). The optical cells were first flushed with prepurified N_2 (Matheson) and then with N_2-saturated buffer. The cells were subsequently filled with deoxygenated buffer, with care taken to remove all bubbles. A small amount of CO-saturated buffer was then injected into the cell through one port, with the small amount of excess buffer released through a vent needle in the second port. Concentrated, deoxygenated hybrid was introduced, and the Mn-containing subunits were reduced with a minimal amount of dithionite. The visible spectra of all samples were monitored throughout the preparative procedures with a Beckman Acta III spectrophotometer.

The CO recombination kinetics were measured with flash photolysis equipment previously described (Stanford et al.,

† From the Department of Chemistry and the Department of Biochemistry, Molecular and Cell Biology, Northwestern University, Evanston, Illinois 60201. *Received June 14, 1983; revised manuscript received January 12, 1984.* This work was supported by Grant HL 13531 from the National Institutes of Health.

* Address correspondence to this author at the Department of Chemistry.

‡ Present address: Laboratory of Chemical Biodynamics, University of California, Berkeley, CA 94720.

[1] Abbreviations: Hb, hemoglobin; [Mn(II),Fe(II)], hemoglobin derivative in which the two chains of a single type, α or β, are substituted with manganese(II) protoporphyrin IX; [Mn(II),Fe(II)(CO)] hybrid, indicates CO ligation of both ferrous chains of a single type; Bis-Tris-HCl, [bis(2-hydroxyethyl)amino]tris(hydroxymethyl)methane hydrochloride; Tris-HCl, tris(hydroxymethyl)aminomethane hydrochloride; MWC, Monod–Wyman–Changeaux model for cooperative ligand binding; T state, low-affinity quaternary conformation of the MWC model; R state, high-affinity quaternary conformation of the MWC model; Hy, unliganded tetrameric hybrid; Hy(CO), monoliganded tetrameric hybrid; $Hy(CO)_2$, diliganded tetrameric hybrid; D, unliganded α,β hybrid dimer; D(CO), monoliganded α,β hybrid dimer.

[2] N. V. Blough, A. Arnone, J. McGourty, and B. M. Hoffman, unpublished results.

0006-2960/84/0423-2883$01.50/0

1980), with either a Sunpak 611 photographic flash or a Xenon Corp. flash lamp, Model 457, screened by a Corning 3-71 filter, as the photolysis sources. The duration of the photographic flash is dependent on the power setting used. Thus, at $^1/_4$ power, the photographic flash exhibits a base line to base line lamp duration of $\sim$650 μs, which decreases to $\sim$200 μs at $^1/_{128}$ power. However, the intensity falls from its maximum to base line in a much smaller time interval, $\sim$75 μs, which is much faster than CO recombination to the hybrids at the low CO concentrations employed. The xenon flash lamp exhibits a base line to base line flash duration of $\sim$20 μs but delivers a lower photon flux and thus could not produce full CO photolysis, as could the photoflash. The actinic light was attenuated with neutral density filters and/or changes in the power setting of the photographic flash.

Under most conditions, the hybrids exhibit biphasic CO recombination kinetics. The following procedure was used to characterize the progress curves. The slow phase isolated by monitoring the decay at long times exhibited pseudo-first-order kinetics, and the pseudo-first-order rate constant for this portion of the slow CO recombination $\bar{k}_s$, was obtained from either a linear least-squares or a nonlinear least-squares fit of the data to an exponential decay. The complete time course of CO recombination was then fit to the sum of two exponentials, eq 1, with one rate constant constrained to be $\bar{k}_s$, by

$$\Delta A(t) = \Delta A_0[F_s e^{-\bar{k}_s t} + (1 - F_s)e^{-\bar{k}_f t}] \quad (1)$$

the use of a nonlinear least-squares fitting routine (Bevington, 1969). Here, F_s is the fraction of heme that recombines with the slow pseudo-first-order rate constant, $\bar{k}_s$, and $\bar{k}_f$ is the rate constant associated with the faster phase. In addition, the first 5–10% of each decay was fit to the first-order expression

$$\Delta A(t) = \Delta A_0 e^{-k_1 t} \quad (1a)$$

Second-order recombination rates k_f, k_s, and k_1 were calculated from the CO pressure and the Henry's law constant S_{CO} = 0.956×10^{-3} M/atm at 25 °C. Where appropriate, the parameters for an individual hybrid with chain i bearing the ferroheme, $i = \alpha$ or β, will be given an additional subscript, namely, k_{fi}, k_{si}, and F_{si}.

Results

This section first presents the kinetic measurements of CO binding subsequent to flash photolytic dissociation of CO from the diliganded [Mn(II),Fe(II)] hybrids and a phenomenological analysis of these results in terms of two-exponential decay function. Next, the data are analyzed within a kinetic formulation of the MWC model for hemoglobin cooperativity, in which T $\rightleftarrows$ R conformational equilibration is assumed to be rapid at each stage of ligation (Hopfield et al., 1971; Parkhurst, 1979). Inadequacies of this formulation lead to the presentation of a model in which equilibration between monoliganded T and R conformers is slow.

Measurement of CO Rebinding Kinetics. Progress curves for CO recombination to the ferrous subunits subsequent to photolysis of [Mn(II),Fe(II)(CO)] hybrids were collected as a function of the photolysis level at pH 6.6, 7.6, 8.0, and 9.0. The traces appear biphasic, as may be seen in representative curves for CO recombination under low (6.6) and high pH (9.0) conditions and at several levels of CO photolysis (P = photolysis fraction) (Figure 1). The progress curves were very well fit to the sum of two exponentials, eq 1, as described above. This description corresponds to CO recombination by two independent sites having different intrinsic binding rates. Although such a model need not apply, as discussed below, the fits to the data are uniformly excellent as seen in Figure 1, and the analysis is extremely useful as a phenomenological characterization of the data.

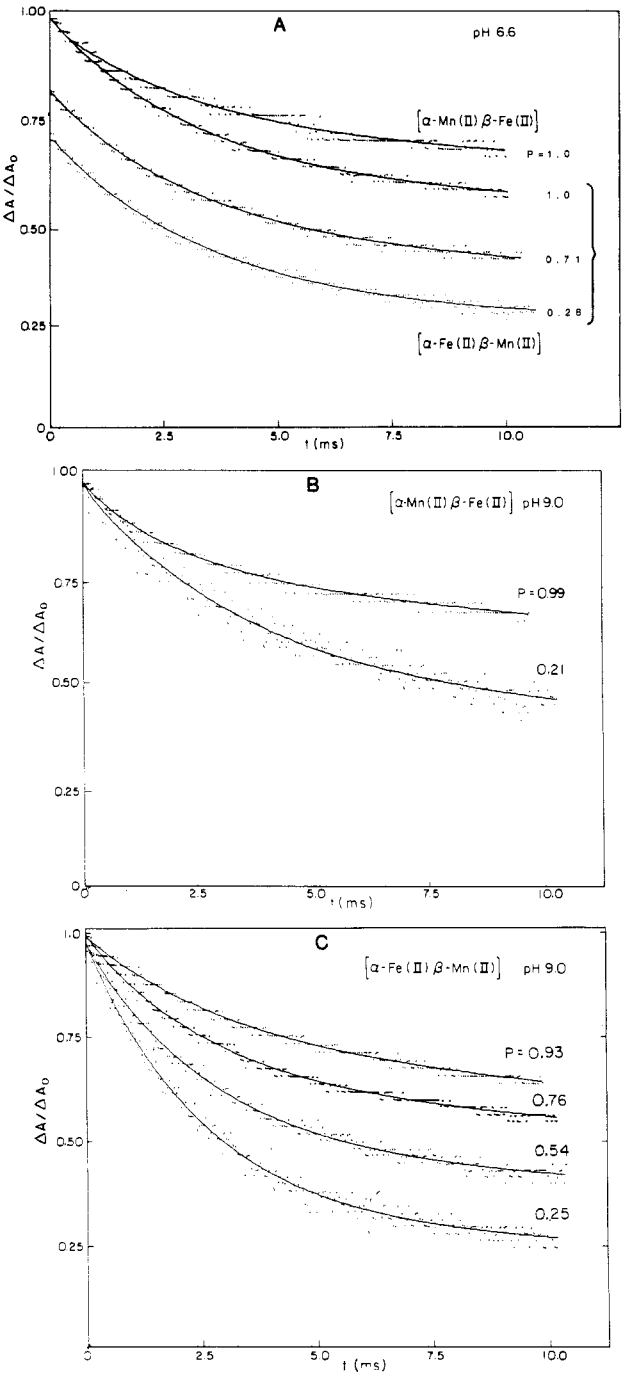

FIGURE 1: Time courses for CO recombination to the [Mn(II),Fe(II)]hybrids: (A) pH 6.6; (B) pH 9.0, $\Delta A/\Delta A_0$, normalized absorption change; P, fraction of photolyzed heme. The recombination was monitored at 436 nm. Heme concentration was $\sim$4 μM in each case, while the CO concentration was 51 μM. Temperature was 23–25 °C. Solid lines represent nonlinear least-squares fits to eq 1, as described under Experimental Procedures. Conditions: (A) pH 6.6, 0.05 M Bis-Tris-HCl, (top trace) [α-Mn(II),β-Fe(II)], (bottom three traces) [α-Fe(II),β-Mn(II)] (Traces at P = 0.71 and 0.28 are offset for clarity); (B) pH 9.0, 0.05 M Tris-HCl, [α-Mn(II),β-Fe(II)]; (C) pH 9.0, 0.05 M Tris-HCl, [α-Fe(II),β-Mn(II)].

The characteristics of the curves depend strongly on conditions. For example, at pH 6.6, the shape of the traces is invariant with photolysis for both hybrids (Figure 1A), but at pH 9.0, the contribution of the fast phase increases as the photolysis level is reduced, particularly for the α-Fe hybrid (Figure 1B,C). The pH and photolysis dependence of F_s, the fraction of hemes that bind CO slowly, is shown in Figure 2.

Table I: Rate Constants for the Fast (k_f) and Slow (k_s) Phases of CO Recombination to the [Mn(II),Fe(II)] Hybrids[a]

pH	hybrid	k_f (μM^{-1} s^{-1})[b] P = 0.1	k_f (μM^{-1} s^{-1})[b] P = 1.0	k_s (μM^{-1} s^{-1}) P = 1.0[c]
6.6	α-Fe	6 (1)	6 (1)	0.15
	β-Fe			0.13
7.6	α-Fe	6 (1)	6 (1)	0.20
	β-Fe			0.15
8.0	α-Fe	6 (1)	6 (1)	0.22
	β-Fe	5.5 (10)	8 (1)	0.20
9.0	α-Fe	6 (1)	6 (1)	0.25
	β-Fe	5.0 (1)	10 (1)	0.29

[a] Progress curves for CO rebinding analyzed according to eq 1. P = photolysis level. Conditions in legend to Figure 1 (0.50 M Tris-HCl or Bis-Tris-HCl, T = 24 ± 1 °C). [b] Here annd in all later tables, parentheses contain the uncertainties in the least significant figure(s). [c] Estimated uncertainty ±0.02 μM^{-1} s^{-1}.

Table II: Concentration Dependence of Fraction of Hybrid Heme That Binds CO Rapidly at Full CO Photolysis (P = 1.0)[a]

pH	hybrid	fraction[b]	[heme] (μM)
6.6	β-Fe	0.27	3.0
		0.47	0.47
		0.54	0.12
	α-Fe	0.37	3.0
		0.50	0.42
9.0	β-Fe	0.20	3.0
		0.45	0.47
		0.68	0.12
	α-Fe	0.21	3.0
		0.42	0.26
		0.50	0.10

[a] Conditions and analysis as in legend to Figure 1. [b] Fraction = 1 − F_s; estimated uncertainty ±0.03.

The rate constants for the fast (k_f) and for the slow (k_s) phases of the α-Fe and β-Fe hybrids are given in Table I. Each is relatively invariant with pH and the fractional photolysis, P, changing at most by a factor of ~2 between pH 6.6 and 9.0, and over the full photolysis range, $0 \leq P \leq 1$. At pH 6.6, the slow-phase rate constants for the individual chains are approximately equal (0.13–0.15 μM^{-1} s^{-1}) and are characteristic of the low-affinity, or T-state CO on-rate for the individual chains within Hb (Parkhurst, 1979; Blough et al., 1980). At pH 6.6, the rate constant for the fast phase (k_f) is the same for both hybrids, $k_s \sim 6$ μM^{-1} s^{-1}, ca. 40-fold greater than that for the slow phase. However, at higher values of pH, the rate constant for the fast phase of CO recombination to the β-Fe hybrid, which increases slightly with pH, also shows a small, but definite increase with increasing level of photolysis. For example, at pH 9.0, $k_{f\beta} \sim 5$ μM^{-1} s^{-1} for ca. 10–20% photolysis, whereas $k_{f\beta} \sim 10$ μM^{-1} s^{-1} at complete photolysis (Table I).

In contrast to the relatively invariant rate constants, the fraction of heme recombining with the slow rate (F_s) and the dependence of F_s on photolysis are strongly affected by pH, particularly for the α-Fe hybrid (Figure 2). For example, at pH 6.6 $F_{s\alpha} \sim 0.6$ and independent of P (Figure 2A), whereas by pH 9.0, $F_{s\alpha} \sim 0.8$ at P = 1 but decreases linearly to $F_s \sim 0.10$ at P = 0.05 (Figure 2D). In comparison, $F_{s\beta}$ shows a significantly strong dependence on P only at pH 9.0 (Figure 2D). Thus, as a first approximation, the major kinetic difference between the two hybrids is observed at alkaline pH: the fraction of material that recombines slowly with CO under low levels of photolysis (F_s) is less for the α-Fe hybrid than for the β-Fe hybrid. However, for Hb at all values of pH, the slowly rebinding phase shows a strong dependence on the photolysis level (May et al., 1975; Schmelzer et al., 1972; Antonini et al., 1967; Gibson, 1959).

Earlier flash photolysis studies on Hb (Gibson & Antonini, 1967; Edelstein et al., 1970; Gray, 1974) and on the Mn(II) hybrids (Blough et al., 1980) indicate that the rapidly recombining phase at complete photolysis represents high-affinity dimers. In order to confirm this interpretation, CO recombination data were collected at complete photolysis under lower heme concentrations, and the results are shown in Table II. Decreasing the heme concentration causes an increase in the fast phase at both pH 6.6 and 9.0, confirming that this phase corresponds to CO recombination by dimers.

All of the above experiments were carried out at a CO concentration of ~50 μM and flash durations from ~300 to 650 μs. To test for competition between CO recombination and the R → T, first-order relaxational process (Sawicki & Gibson, 1976; Gibson, 1959), the recombination kinetics were measured as a function of CO concentration and flash duration. Increasing the CO concentration by a factor of 20, to ~1 mM, and decreasing the flash duration by a factor of ~10, to ~20 μs, did not significantly affect the percentage of the slow phase at pH 6.6 or 9.0. In sharp contrast, for Hb, the fraction of material recombining slowly with CO subsequent to photolysis decreases with increasing CO concentration (Gibson, 1959). The result for Hb is thought to represent a kinetic competition between CO binding and R → T relaxation (Sawicki & Gibson, 1976; Gibson, 1959). The absence of observed effects for the hybrids could be interpreted as indicating either that the rate of conformational equilibration for the hybrids is faster than the fastest rate for CO recombination (6000 s^{-1}) or is much slower than the fastest rate at both pH 6.6 and 9.0. The latter explanation is to be preferred, as is justified presently.

For use in the analysis of the next section, initial CO recombination rates (k_1) also were acquired by fitting the first 5–10% of each decay to the first-order expression, eq 1a. Representative plots of k_1 vs. P are shown in Figure 3 for the α-Fe hybrid, and the slope (S) and intercept (I) data provided by these plots are given in Table III.

Table III: Initial Rate (S and I)[a] and Kinetic MWC Parameters[b] for CO Binding to the [Mn(II),Fe(II)] Hybrids[c]

	α-Fe						β-Fe					
pH	S	I	k_1[d]	k_D[e]	F[f]	k_2[g]	S	I[h]	k_1[d]	k_D[e]	F[d]	k_2[g]
6.6	−0.21 (2)	2.3 (4)	0.15	6	0.63	0.13 [0.41]	0.63 (2)	1.2	0.13	6	0.73	[i]
7.6	−1.3 (3)	2.5 (4)	0.20	6	0.84	1.8 [1.6]	−0.0 (2)	1.8	0.15	6	0.75	0.40 (3) [0.16 (4)]
8.0	−3.0 (3)	3.8 (5)	0.22	6	0.84	3.4 [3.7]	−0.4 (2)	2.0	0.20	8	0.80	0.50 (3) [0.61 (5)]
9.0	−4.8 (4)	6.1 (5)	0.25	6	0.79	6.1 [6.2]	−1.1 (3)	2.9	0.29	10	0.79	1.1 (4) [1.5 (5)]

[a] Slope (S) and intercept (I) obtained from plots (e.g., Figure 3) of initial rate (k_1) vs. percent photolysis (P). [b] Defined in Figure 3 and eq 2 and 3. [c] Parameters are rate constants with dimensions μM^{-1} s^{-1}, unless noted. [d] Uncertainty ±0.02. [e] Uncertainty ±1. [f] Dimensionless (eq 3); uncertainty ±0.03. [g] Values calculated from eq 6a; values in brackets, from eq 6b (see text). [h] Uncertainty ±0.4. [i] The calculations gave negative values for k_2 (−0.58 and [−0.78]).

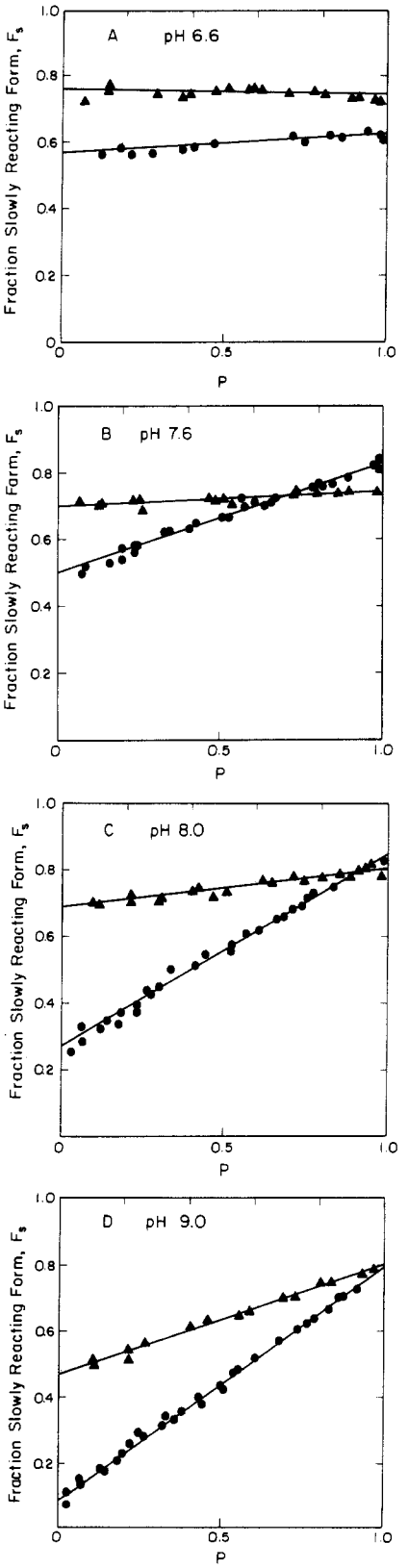

FIGURE 2: Effect of pH and the photolysis level (P) on F_s, the fraction of [Mn(II),Fe(II)] hybrid heme slowly recombining with CO (eq 1): [α-Mn(II),β-Fe(II)] (▲); [α-Fe(II),β-Mn(II)] (●). Conditions are described in Figure 1. (A) pH 6.6, 0.05 M Bis-Tris-HCl buffer; (B) pH 7.6, 0.05 M Tris-HCl buffer; (C) pH 8.0, 0.05 M Tris-HCl buffer; (D) pH 9.0, 0.05 M Tris-HCl buffer.

Kinetic MWC Model Fitting. When two ligands bind to one of the [Mn(II),Fe(II)] hybrids, it corresponds to a particular microscopic sequence by which Hb binds its first two ligands (Blough & Hoffman, 1984) and the process can be represented within the MWC model by the reaction scheme

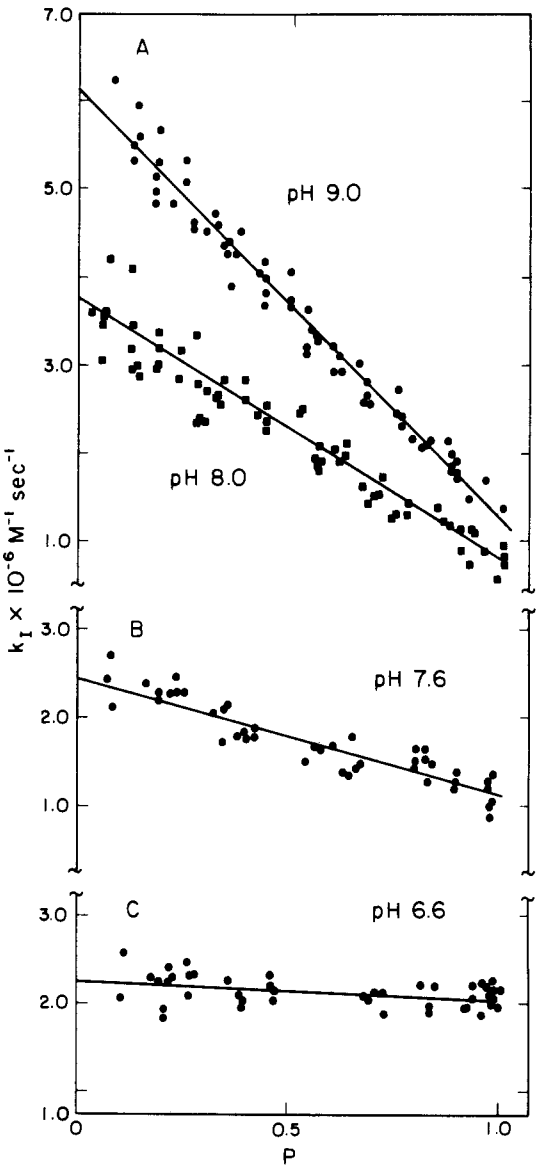

FIGURE 3: Effect of pH and photolysis level on the initial rates for CO recombination to the [α-Fe(II),β-Mn(II)] hybrid k_I (eq 1a). The solid lines represent linear least-squares fits of the data; the slopes, S, and intercepts, I, are listed in Table III. Conditions are described in Figures 1 and 2. (A) pH 9.0 (●), pH 8.0 (■); (B) pH 7.6; (C) pH 6.6.

in Figure 4. The squares represent the T-state form of Hb, which combines with CO at a slow rate, characterized by the microscopic rate constant k_T and the circles represent the R state, which rapidly combines CO, characterized by the rate constant k_R. The semicircles represent dimers that bind CO rapidly with a rate constant $k_D \sim k_R$ (Gibson & Antonini, 1967; Edelstein et al., 1970; Gray, 1974). The allosteric constant, L_0, is the concentration ratio of the low- to high-affinity structures for unliganded Hb and at low pH is of the order 10^5–10^6 for the Mn(II) hybrids (Blough & Hoffman, 1984), as for Hb (Baldwin, 1975). The allosteric constants for liganded forms are $L_j = L_0C^j$, where j indicates the number of ligands bound and C is the ratio of CO dissociation constants for the high- to low-affinity structures. K_{42} is the R-state tetramer to dimer dissociation constant.

Before a photolyzing flash, the hybrids exist as an equilibrium mixture of diliganded tetramers and monoliganded dimers (Figure 4). If it is assumed that the R → T relaxation after the flash is rapid with respect to CO binding and that equilibration between the T and R forms is faster than CO

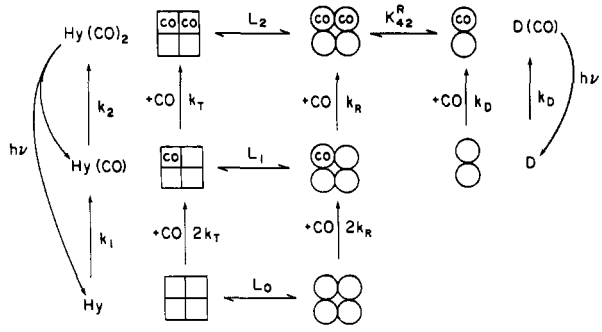

FIGURE 4: Scheme for the kinetic MWC model. Squares represent the T-state form of the [Mn(II),Fe(II)] hybrids, which recombines with CO at a slow rate characterized by the microscopic rate constant k_T, and the circles represent the R-state form, which rapidly recombines with CO with the rate constant k_R. Semicircles represent dimers that bind CO rapidly with the rate constant k_D. Other parameters are defined in the text. Before photolysis, the hybrids exist as an equilibrium mixture of diliganded tetramers and liganded dimers. After full photolysis, only unliganded tetramer, Hy, and dimer, D, are present; otherwise, the monoliganded tetramer, Hy(CO), also is formed. If R $\rightleftarrows$ T equilibration is rapid as compared to CO binding, this kinetic scheme reduces to an Adair model, where k_1 and k_2, given in eq 2, are the rate constants for CO binding to Hy and Hy(CO), respectively.

binding during the recombination process, the hybrid CO binding kinetics reduces to an Adair model whose rate constants can be expressed in terms of the microscopic MWC parameters (Hopfield et al., 1971; Parkhurst, 1979). Here

Scheme I

$$\mathrm{Hy} + 2\mathrm{CO} \underset{h\nu}{\overset{k_1}{\rightleftharpoons}} \mathrm{Hy(CO)} + \mathrm{CO} \underset{h\nu}{\overset{k_2}{\rightleftharpoons}} \mathrm{Hy(CO)_2}$$

$$\mathrm{D} + \mathrm{CO} \underset{h\nu}{\overset{k_D}{\rightleftharpoons}} \mathrm{D(CO)}$$

$$k_1 = 2[f_0 k_T + (1 - f_0)k_R]$$

$$k_2 = [f_1 k_T + (1 - f_1)k_R] \quad (2)$$

$$f_j = \frac{[T]_j}{[T]_j + [R]_j} = \frac{L_0 C^j}{L_0 C^j + 1} \quad (2a)$$

the effective rate constants for CO binding to the unliganded (Hy) and monoliganded [Hy(CO)] tetrameric hybrids are k_1 and k_2, respectively, and are given by a linear combination of the microscopic MWC rate constants k_T and k_R (eq 2). The fraction of tetrameric hybrid in the T state at the jth binding step is given by f_j. The subscript i, which identifies the type of the ferrous chain in a hybrid, has been suppressed for clarity. Dimer association does not occur on the time scale of these measurements (Andersen et al., 1971; Wiedermann & Olsen, 1975), and thus, the rapid CO binding by dimers, with rate constant k_D, is included as a parallel reaction. Scheme I represents a sequential two-step, irreversible binding of CO to tetrameric forms of the protein, upon which is superimposed the independent, single-step binding by dimers. With the convenient, but unnecessary (see paragraph at end of paper regarding supplementary material), assumption of equal quantum yields for the R, T, and dimer forms, an analytical solution to the differential equations describing the time course of the absorbance excursion during CO recombination and subsequent to fractional photolysis, P, is readily obtainable (Rodiguin & Rodiguina, 1964). With the fraction of hybrid in the tetrameric form denoted F, the dimer (D) contribution to the time course of CO recombination is given by

$$\Delta A_d(t) = \Delta A_0(1 - F)Pe^{-k_D t} \quad (3)$$

while the tetramer contribution [Hy and Hy(CO)] is given by

$$\Delta A_t(t) = \Delta A_0 PF\left(P\left[1 + \frac{k_1}{2(k_2 - k_1)}\right]e^{-k_1 t} + \left(1 - P\left[1 + \frac{k_1}{2(k_2 - k_1)}\right]\right)e^{-k_2 t}\right) \quad (3a)$$

and the complete time course of the absorption excursion is the sum of the dimer and tetramer contributions:

$$\Delta A(t) = \Delta A_t(t) + \Delta A_d(t) \quad (4)$$

Here, ΔA_0 is the total absorption excursion at full photolysis.

Initial rate measurements can be used to facilitate the process of analyzing the kinetic data for the hybrids. Expanding the exponentials within eq 4 and keeping only terms linear in t lead to an algebraic expression for the observed initial rate, k_I (Figure 3, Table III), as a function of photolysis:

$$k_I = k_2 F + k_D(1 - F) + [F(k_1/2 - k_2)]P \quad (5)$$

This equation predicts a linear dependence of the initial rates on photolysis, with the slope (S) and intercept (I) given by

$$S = -(F/2)(2k_2 - k_1) \quad (6a)$$

$$I = Fk_2 + (1 - F)k_D \quad (6b)$$

As will be seen, a value for each of the four parameters, k_1, k_2, k_D, and F, can be obtained by combining the results from two-exponential fits to progress curves at full photolysis (P = 1) with the values of S and I (Table III).

The simplest situation described by this kinetic model arises when both the monoliganded HyCO and the unliganded Hy species produced by photolysis each fully adopts the T state; this corresponds to equilibrium ratios $L_0 \gg 1$ and $L_1 = L_0 C \gg 1$. A two-exponential recombination process is predicted by eq 4; the HyCO and Hy tetramers bind slowly, with rate constant k_T, the dimers bind rapidly, with rate constant k_D, and the fraction of the slow phase and the initial rate is independent of P. The α-Fe hybrid at pH 6.6 and the β-Fe hybrid at pH $\leq$ 8 behave in this fashion (Figures 1A, 2, and 3), with the two-exponential fits and initial rates varying only minimally with photolysis. The fast (k_f) and slow (k_s) phase rate constants directly measured thus correspond to k_D and k_T (Table III), and the fraction of slow phase corresponds to F, the fraction of tetrameric protein.

More generally, the shape of a CO recombination trace varies with the photolysis level, P. The α-Fe hybrid at pH 9 represents an extreme (Figure 1C), with the fraction of the slowly binding component linearly approaching near to zero as $P \rightarrow 0$ (Figure 2D). This particular characteristic can be described by eq 3–6. When the unliganded hybrid Hy is fully in the T state, but there is already substantial or complete T or R conversion even after the first ligand, the inequality $k_1 \ll k_2$ applies (eq 2). In this case, CO recombination to tetrameric hybrid subsequent to full photolysis (P = 1) appears as a slow monophasic process (eq 3a), with $k_s = k_1$, because CO binding to T-state Hy is rate limited by the first, slow binding step. Since dimers bind rapidly (eq 3), the overall binding process is biphasic (eq 4), with the fast and slow phases reflecting dimer and tetramer CO recombination, respectively. When photolysis is not complete, $P < 1$, both Hy and Hy(CO) are formed during the flash and CO recombination to tetrameric hybrid is itself biphasic; Hy is completely in the T state and recombines slowly with rate constant k_1, whereas Hy(CO) is largely in the R-state and reacts rapidly with rate constant

k_2. Since the R-state and dimer rate constants are comparable, $k_D \sim k_2$, the complete time course of CO recombination (eq 4) will be closely approximated by a two-exponential process: Both D and Hy(CO) contribute to the fast phase, Hy to the slow phase. Equation 3a then predicts that the slow binding phase, which is proportional to the concentration of Hy produced by the flash, will vanish as $P \rightarrow 0$, much as is observed for the α-Fe hybrid at pH 9 (Figures 1C and 2D).

For the general case in which the shape of a CO recombination trace varied with P, namely, for the α-Fe hybrid at pH > 6.6 and for the β-Fe hybrid at pH 9.0, attempts to parameterize Scheme I employed the following procedure. On the basis of the discussion following eq 3 and 4, the rate constant k_1 can be associated with that for the slow phase, k_s, given in Table II. The fraction of tetramer, F, and the dimer rate constant, k_D, were assigned as the fraction of slow component and the rate constant for the rapid component from an analysis of the biphasic decay traces at full photolysis ($P = 1$), according to eq 1, holding k_1 fixed. The values for k_1, F, and k_D at each pH are collected in Table III. Finally, the CO on-rates for the monoliganded hybrid, k_2, were calculated from the initial rate data and the estimates for F and k_D from both eq 6a and 6b; the two values are in good agreement (Table III), indicating the analysis to be internally consistent. As a stringent test on the model, these four MWC parameters were then used in eq 4 to represent the family of complete progress curves obtained as a function of P.

Following this procedure, when F, k_D, and k_1 were held constant and k_2 was optimized, the complete set of decay curves for the α-Fe hybrid at pH 9.0 (Figure 5A) could be fit rather well with the single value of k_2 initially obtained from eq 6. Thus, for this case, both the initial rate data and the complete set of progress curves can be well represented by eq 4 with a single set of parameters.

Attempts to fit the data for the β-Fe hybrid at pH 9 were less successful. The values of k_D, F, and k_2 obtained by the procedure described above did not permit a reasonable representation of the full family of progress curves. Although a systematic variation of k_D and F did give one set of values that allowed such a representation ($F = 0.74$; $k_D = 8.3\ \mu M^{-1}\ s^{-1}$; $k_1 = 0.29\ \mu M^{-1}\ s^{-1}$; $k_2 = 1.1\ \mu M^{-1}\ s^{-1}$), these values did not reproduce the initial rate parameter S.

Most importantly, the kinetic MWC expressions totally fail to reproduce the experimental data for the α-Fe hybrid at pH values of 7.6 and 8. No set of values for k_D, k_2, and F reproduces both the initial rate data and the full recombination time course at all levels of photolysis. This latter difficulty is displayed in Figure 5B,C, which give decay traces and the wholly inadequate, theoretical progress curves obtained from eq 4 by using parameters derived from same procedures employed above. The theory reproduces the data reasonably well at high P, but systematic deviations arise as P is lowered. In particular, as photolysis decreases, the theoretical progress curves correspond to a larger proportion of fast-reacting material than do the actual data. This trend is also apparent for the α-Fe hybrid at pH 9.0 (Figure 5A), although the deviations are much smaller.

The discrepancy between the experimental results for the α-Fe hybrids at pH 7.6 and above and the corresponding predictions of the kinetic MWC equations can be understood as follows. With a very weak actinic flash, at most a single CO is dissociated from the diliganded, tetrameric hybrid, producing the Hy(CO) intermediate. If this species undergoes rapid equilibration between its T and R forms, it should rebind CO with the composite rate constant k_2 (eq 2). However,

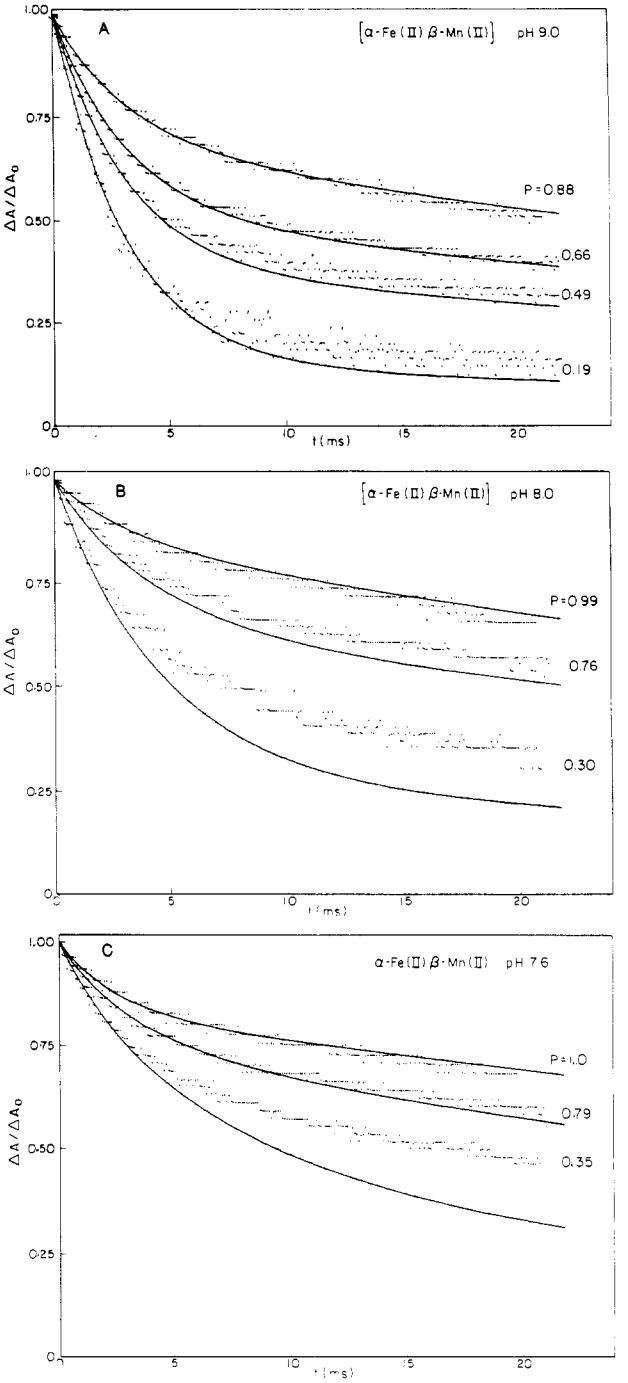

FIGURE 5: Time course for CO recombination to the [α-Fe(II),β-Mn(II)] hybrids. Solid lines represent predictions of the MWC model, eq 4, with optimized kinetic parameters, differing only slightly from those of Table III. Experimental traces were acquired under the conditions described in Figures 1 and 2. (A) pH 9.0; MWC kinetic parameters are $F = 0.78$, $K_D = 6.03\ \mu M^{-1}\ s^{-1}$, $k_1 = 0.25\ \mu M^{-1}\ s^{-1}$, and $k_2 = 6.1\ \mu M^{-1}\ s^{-1}$. (B) pH 8.0; MWC kinetic parameters are $F = 0.84$, $k_D = 5.4\ \mu M^{-1}\ s^{-1}$, $k_1 = 0.22\ \mu M^{-1}\ s^{-1}$, and $k_2 = 3.6\ \mu M^{-1}\ s^{-1}$. (C) pH 7.6; MWC kinetic parameters are $F = 0.82$, $k_D = 7.0\ \mu M^{-1}\ s^{-1}$, $k_1 = 0.20\ \mu M^{-1}\ s^{-1}$, and $k_2 = 1.7\ \mu M^{-1}\ s^{-1}$.

analysis of the initial rates and the progress curves at full photolysis gives values for k_2 that are large and comparable to the dimer rate, $k_2 \sim k_D \sim 10^6\ M^{-1}\ s^{-1}$ (Table III). Therefore, the Hy(CO) tetramers and unliganded dimers, which are the only photolysis products as the flash intensity approaches zero, both should bind CO rapidly. In consequence, the progress curves are predicted to become monophasic and fast as $P \rightarrow 0$. The same conclusion was reached above in the general analysis of eq 4 for the case $k_2 \sim k_D \gg k_1$, which applies here.

Table IV: Allosteric Equilibrium Constants for the Unliganded, Monoliganded, and Diliganded [Mn(II),Fe(II)] Hybrid Hb[a]

	α-Fe		β-Fe	
pH	L_2	L_2^K	L_2	K_2^K
6.6	≥12	8[b]	≥9.0	>10
7.6	1.7 (5)	1.3 (5)	≥5.8	>10
8.0	0.6 (5)	0.5 (2)	0.7 (6)	6.3 (42)
9.0	0.08 (6)	0.10 (8)	0.4 (3)	1.4 (5)

[a] L_2 is calculated from equilibrium CO binding data of Blough & Hoffman (1984); K_2^K is calculated from kinetic data as described in text. [b] Order of magnitude estimate.

In short, for the cases in question, a large fraction of slowly recombining phase in experiments where the photolysis level approaches zero, $P \rightarrow 0$ (Figure 2), is incompatible with the kinetic MWC model, for the latter requires that the fraction of slow recombination vanish, $F_s \rightarrow 0$ as $P \rightarrow 0$. Although the known differences between the quantum yields of the T and R states, with $\phi_T > \phi_R$ (Sawicki & Gibson, 1979), will bias the relative populations of photolysis products, Hy, Hy-(CO), and D, in a fashion to favor Hy, and thus increase F_s, calculations incorporating these differences show that the effect is far too small to explain the discrepancies (see paragraph at end of paper regarding supplementary material).

Slow-Conversion MWC Model. Instead, the kinetic results can be explained if the interconversion between the T and R forms of the monoliganded photolysis intermediate, Hy(CO), is slow compared to CO recombination with the R form (ca. 300–500 s^{-1}). This is in contrast to the rapid R → T relaxation of the unliganded tetramer, which appears to be much faster than CO binding (Table IV, eq 2a), as indicated by the large proportion of the progress curve that exhibits the slow, T-state rate at full photolysis ($P = 1$). This latter conclusion was first reached by Sawicki & Gibson (1976).

The kinetic data can be described by a simple heuristic application of MWC principles with allowance for restricted quaternary structure interconversion. In this model, unliganded tetramer produced by photolysis converts rapidly and completely ($L_0 \gg 1$) to the stable, T-state structure; subsequently, it rebinds CO slowly, with a rate constant of approximately k_T. In contrast, photorelease of one ligand from the diliganded tetrameric species, $Hy(CO)_2$, produces tetrameric, monoliganded Hy(CO) intermediates that do *not* rapidly interconvert between T and R forms; the ratio between monoliganded quaternary structures, $L_1 = [T]_1/[R]_1$, remains at the equilibrium value of the diliganded tetramer; $L_1 = L_2 \equiv ([T]_2/[R]_2)_{eq}$. In the absence of equilibration between the monoliganded T_1 and R_1 species, they independently rebind CO at the slow, T-state (k_T) and fast, R-state (k_R) intrinsic rate constants, respectively. In addition, dimers that have lost CO will rebind it at the fast rate, $k_D \sim k_R$ (Gray, 1974; Edelstein et al., 1970; Gibson & Antonini, 1967). If one ignores, for simplicity, the unequal quantum yields for the T, R, and D species, this model gives the following expression for the time course of the absorption excursion at fractional photolysis, P:

$$\Delta A(t) = \Delta A_0 P[F([P(1-f_2)+f_2]e^{-k_T t} + (1-P) \times (1-f_2)e^{-k_R t}) + (1-F)e^{-k_D t}] \quad (7)$$

At equilibrium (before photolysis), $1 - F$ is the fraction of dimer and f_2 is the fraction of diliganded tetramer, $Hy(CO)_2$ (eq 2), in the T state. Because $k_R \sim k_D$, eq 7 reduces to the sum of two exponentials under all conditions of P and f_2. Thus, it is equivalent to eq 1 and fully reproduces the kinetic traces under all conditions (Figure 1).

Table V: Rate Constant (k_R) for CO Binding to the Monoliganded R-State [Mn(II),Fe(II)] Hybrids[a]

pH	hybrid	k_R (μM^{-1} s^{-1})[b]
9.0	α-Fe	7.0 [6.8]
	β-Fe	3.6 [2.2]
8.0	α-Fe	5.4 [4.8]
	β-Fe	3.8 [2.3]
7.6	α-Fe	3.8 [3.4]
	β-Fe	

[a] Calculated from eq 9, as described in the text. Rate constants for CO binding to the T-state hybrids are equal to the slow-phase rate constants given in Table I ($k_T = k_s$). [b] Values calculated from eq 9a; those in brackets, from eq 9b. See footnote 3.

Equation 7 predicts a linear dependence of the initial rates on photolysis level P:

$$k_I = k_D(1-F) + F[(1-f_2)k_R + f_2 k_T] + F[(1-f_2)k_T - (1-f_2)k_R]P \quad (8)$$

with the slope (S) and intercept (I) given by

$$I = k_D(1-F) + F[(1-f_2)k_R + f_2 k_T] \quad (9a)$$

$$S = -F[k_R(1-f_2) - k_T(1-f_2)] \quad (9b)$$

However, unlike the equations arising from Scheme I, these equations are consistent with a finite proportion of slowly reacting hemes at low photolysis ($P \rightarrow 0$). Moreover, they correctly predict the linear dependence of the slow phase percentage on photolysis (Figure 2). The fraction of the slow phase at full photolysis, $P = 1$, corresponds to the fraction of tetrameric protein ($F_s = F$); the $P \rightarrow 0$ intercept of a plot of the slowly recombining fraction (F_s) vs. photolysis fraction corresponds to diliganded T-state tetramer prior to photolysis ($F_s = Ff_2$). With f_2 thus calculable, the model provides a kinetic estimate for the ratio $L_2 = [T]_2/[R]_2$ (eq 2a); the values for these ratios are given as L_2^K in Table IV. At every pH, the value of L_2^K obtained for the α-Fe hybrid by this analysis is in excellent agreement with L_2, the corresponding value obtained from equilibrium CO binding measurements (Table IV). The values of L_2^K and L_2 for the β-Fe hybrid do not match quite as well, although L_2^K still is much closer to the L_2 than to the L_1 obtained in the equilibrium measurements (Blough & Hoffman, 1984). The slow conversion model thus not only provides a good description of the kinetics of CO binding but also reconciles the equilibrium and kinetic CO binding data.

Analysis of the kinetic data within this model indicates that both hybrids remain largely in the T state through two ligand binding steps at pH 6.6, but at higher pH the hybrids show significant conversion to the R state after the second ligand is bound (Table IV, Figure 2). Above pH ~7.6, conversion to the R state is substantially greater for the α-Fe hybrid than for the β-Fe, in support of earlier equilibrium measurements (Blough & Hoffman, 1984). For example, at pH 7.6, only 10% of the diliganded [α-Mn(II),β-Fe(II)(CO)] hybrid converts to the R quaternary structure but ~40% of the [α-Fe-(II)(CO),β-Mn(II)] hybrid does so (Table IV, eq 2). By pH 9.0, these percentages have increased to ~40% for the β-Fe hybrid and 90% for the α-Fe hybrid.

Since there appears to be no quaternary structure change when Hy(CO) is generated by the photolysis of a single ligand from $Hy(CO)_2$, the parameter k_R in eq 7–9 represents that of the monoliganded, Hy(CO) intermediate. Its value can be calculated from eq 9, with the slope (S) and intercept (I) of a plot of initial rate vs. photolysis (Figure 3, Table III);[2] results are presented in Table V.[3] The rate constant for binding to

the T state, k_T, is equal to that for the slow component in a two-component fit to the progress curves; the values are given in the last column of Table I ($k_T = k_s$).

At pH 9.0, the on-rate for α-Fe in a monoliganded, R-state tetramer is $k_R \sim 7\ \mu M^{-1}\ s^{-1}$, about twice that of β-Fe. Decreasing the pH to 7.6 halves k_R for α-Fe, whereas k_R for the β-Fe hybrid remains constant. These rates for binding a second CO to the R-state tetramer are not as large nor do they exhibit the same pH dependence as those we report elsewhere for adding the fourth CO to the R-state [e.g., Table III in Blough & Hoffman (1984)]. In particular, k_R for the β chain within the monoliganded R state is ~2–3-fold lower than that for the triliganded R state at pH values of both 8.0 and 9.0 (Blough & Hoffman, 1984; DeYoung et al., 1976). These differences are small compared to the differences between the T and R states but do suggest that the R state has slightly different properties at the monoliganded and triliganded ligation level. In short, they suggest a small degree of direct subunit interaction.

Discussion

The kinetic measurements on the [Mn(II),Fe(II)] hybrid hemoglobins provide a full pH dependence of the CO binding rate constants for both α- and β-Fe chains within the T state and, at elevated values of pH, give the monoliganded R-state rate constants as well. The measurements further indicate that binding CO to the α chains produces greater T → R conversion than binding to β, in support of our equilibrium measurements of CO binding (Blough & Hoffman, 1984).

For those conditions in which the hybrid CO recombination kinetics remain independent of photolysis, namely, pH 6.6 for the α-Fe hybrid and pH ≤ 8.0 for the β-Fe, the two kinetic formulations of the MWC model describe the experimental results equally well. However, the rapid equilibration model would indicate that the tetramer is completely in the T state when zero or one CO is bound, whereas the slow conversion model also requires that the diliganded tetramer is predominantly in the T state. Since equilibrium CO binding measurements at low pH show that the diliganded hybrids are in fact predominantly in the T state at low pH (Blough & Hoffman, 1982, 1984), they provide some support for the slow conversion kinetic scheme.

However, at higher pH, the assumption of rapid T–R equilibration at all early stages of Hb ligation clearly fails. Instead, the results indicate that T → R conversion of the unliganded tetramer is rapid compared to its CO binding rate, but the reverse holds when a a single ligand is bound. NMR (Ogawa & Shulman, 1971, 1972; Cassoly et al., 1971), kinetic (Cassoly & Gibson, 1972), and pulse radiolysis (Rollema & deBruin, 1978) studies on the valency hybrids argue that T → R interconversion is slow at the diliganded level, as well. For example, Rollema & deBruin (1978) suggest that the immediate product of complete pulse radiolytic reduction of [Fe(CO),Fe(III)] valency hybrids rapidly partitions into noninterconverting T_2 and R_2 diliganded forms. Our results indicate that R → T conversion at the monoliganded stage is even more restricted. The good correspondence between the value of L_2 derived from kinetic and from equilibrium measurements with the α-Fe(II) hybrid (Table IV) suggests that the rate for $R_1 \rightarrow T_1$ conversion is much less than that for binding a second CO to R_1 (300–500 s^{-1}).

Thus, studies of discrete intermediates representing various Hb ligation stages give evidence of slow quaternary structure interconversion in mono- and diliganded tetrameric hemoglobins. This body of results is in agreement with those of Sawicki & Gibson (1976), who employed a kinetic MWC model to analyze the R → T relaxation in Hb subsequent to a short actinic pulse, insofar as they conclude that the R → T relaxation is rapid for the formation of the unliganded species. However, their conclusion that the R → T relaxation is rapid compared to CO binding at intermediate ligation stages stands in *apparent* contradiction. Several obvious resolutions may be suggested. One is that the conversion observed by Sawicki and Gibson proceeds through intermediate species not accessible in any of the hybrid analogues. A second is that the stable diliganded intermediate in the form of a hybrid differs from the transient diliganded intermediate produced by photolysis. These suggestions and variants have the common feature that they require a plasticity of structures within a given quaternary state at a particular ligation level. That is, they support the conclusions of Sawicki and Gibson that a rigid two-state interpretation of the Hb kinetics is inappropriate. This conclusion is further supported by differences in R-state on-rates at the monoliganded level reported here.

Supplementary Material Available

Analysis of the effects of differences between the quantum yield in the T and R states on the observed kinetics (3 pages). Ordering information is given on any current masthead page.

Registry No. CO, 630-08-0; Mn, 7439-96-5.

References

Andersen, M. E., Moffat, J. K., & Gibson, Q. H. (1971) *J. Biol. Chem. 246*, 2796–2807.

Antonini, E., Chiancone, E., & Brunori, M. (1967) *J. Biol. Chem. 242*, 4360–4366.

Baldwin, J. M. (1975) *Prog. Biophys. Mol. Biol. 29*, 225–320.

Bevington, P. R. (1969) *Data Reduction and Error Analysis for the Physical Sciences*, McGraw-Hill, New York.

Blough, N. V., & Hoffman, B. M. (1982) *J. Am. Chem. Soc. 104*, 4247–4250.

Blough, N. V., & Hoffman, B. M. (1984) *Biochemistry* (previous paper in this issue).

Blough, N. V., Zemel, H., Hoffman, B. M., Lee, T. C. K., & Gibson, Q. H. (1980) *J. Am. Chem. Soc. 102*, 5683–5685.

Cassoly, R., & Gibson, Q. H. (1972) *J. Biol. Chem. 247*, 7332–7341.

Cassoly, R., Gibson, Q. H., Ogawa, S., & Shulman, R. G. (1971) *Biochem. Biophys. Res. Commun. 44*, 1015–1021.

Edelstein, S. J., Rehmar, M. J., Olsen, J. S., & Gibson, Q. H. (1970) *J. Biol. Chem. 245*, 4372–4381.

Gibson, Q. H. (1959) *Biochem. J. 71*, 293–303.

Gibson, Q. H., & Antonini, E. (1967) *J. Biol. Chem. 242*, 4678–4681.

Gray, R. D. (1974) *J. Biol. Chem. 249*, 2870–2885.

Hoffman, B. M., & Gibson, Q. H. (1978) *Proc. Natl. Acad. Sci. U.S.A. 75*, 21–25.

Hopfield, J. J., Shulman, R. G., & Ogawa, S. (1971) *J. Mol. Biol. 61*, 425–443.

May, R. P., & Mayer, A. (1975) *Eur. J. Biochem. 52*, 589–593.

Ogawa, S., & Shulman, R. G. (1971) *Biochem. Biophys. Res. Commun. 42*, 9–16.

[3] The calculation is feasible in situations where $S > 0$. F and f_2 are obtained from the high and low photolysis intercepts when one plots the slowly combining fraction vs. P (Figure 2), and k_T is taken to be the appropriate value of k_s from Table III. Estimates of k_R calculated from eq 9b are shown in Table V, accompanied by those calculated from eq 9a (given in parentheses). The values for k_R from the two equations are in good agreement, which demonstrates that the treatment is internally consistent.

Ogawa, S., & Shulman, R. G. (1972) *J. Mol. Biol. 70*, 315–336.
Parkhurst, L. J. (1979) *Annu. Rev. Phys. Chem. 30*, 503–546.
Rodiguin, N. M., & Rodiguina, E. N. (1964) *Consecutive Chemical Reactions: Mathematical Analysis and Development* (Schneider, H., Ed.) Van Nostrand, New York.
Rollema, H. S., & deBruin, S. H. (1978) *Eur. J. Biochem. 83*, 313–317.
Sawicki, C. A., & Gibson, Q. H. (1976) *J. Biol. Chem. 251*, 1553–1542.
Sawicki, C. A., & Gibson, Q. H. (1977) *J. Biol. Chem. 252*, 7538–7547.
Sawicki, C. A., & Gibson, Q. H. (1979) *J. Biol. Chem. 254*, 4058–4062.
Schmelzer, U., Steiner, R., Mayer, A., Nedetzka, T., & Fasold, H. (1972) *Eur. J. Biochem. 25*, 491–497.
Stanford, M. A., Swartz, J. C., Phillips, T. E., & Hoffman, B. M. (1980) *J. Am. Chem. Soc. 102*, 4492–4499.
Wiedermann, B. L., & Olsen, J. S. (1975) *J. Biol. Chem. 250*, 5273–5275.

Structural and Functional Properties of Calmodulin from the Eukaryotic Microorganism *Dictyostelium discoideum*†

Daniel R. Marshak, Margaret Clarke, Daniel M. Roberts, and D. Martin Watterson*

ABSTRACT: Calmodulin was purified from the eukaryotic microorganism *Dictyostelium discoideum* and characterized in terms of its nearly complete primary structure and quantitative activator activity. The strategy for amino acid sequence analysis took advantage of the highly conserved structure of calmodulin and employed a new procedure for limited cleavage of calmodulin that uses a protease from mouse submaxillary gland. Fourteen amino acid sequence differences between *Dictyostelium* and bovine calmodulin were identified unequivocally, as well as an unmethylated lysine at residue 115 instead of N^{ϵ},N^{ϵ},N^{ϵ}-trimethyllysine. Seven of the amino acid substitutions in *Dictyostelium* calmodulin are novel in that the residues at these positions are invariant in all calmodulin sequences previously examined, most notably an additional residue at the carboxy terminus. Comparison of the *Dictyostelium* calmodulin sequence with other calmodulin sequences shows that the region with the greatest extended sequence identity includes parts of the first and second structural domains and the interdomain region between domains 1 and 2. *Dictyostelium* calmodulin activated bovine brain cyclic nucleotide phosphodiesterase in a manner indistinguishable from that of bovine brain calmodulin. However, *Dictyostelium* calmodulin activated pea NAD kinase to a maximal level 4.6-fold greater than that produced by bovine brain calmodulin. This functional difference demonstrates the potential biological importance of the limited number of amino acid sequence differences between *Dictyostelium* calmodulin and other calmodulins and provides further insight into the structure, function, and evolution of the calmodulin family of proteins.

Calmodulin is a calcium binding protein that has been found in all eukaryotic cells examined in detail. It has multiple in vitro biochemical activities and has a highly conserved primary structure [for recent reviews, see Klee & Vanaman (1982) and Burgess et al. (1983)]. Complete amino acid sequences are available for calmodulin from bovine brain (Watterson et al., 1980a, 1984) and human brain (Sasagawa et al., 1982). Nearly complete sequences have been reported for calmodulin from rabbit skeletal muscle (Grand et al., 1981), rat testis (Dedman et al., 1978), scallop muscle (Toda et al., 1981), *Metridium senile* (Takagi et al., 1980), *Tetrahymena pyriformis* (Yazawa et al., 1981), *Renilla reniformis* (Jamieson et al., 1980), and spinach leaf (Burgess et al., 1983; Watterson et al., 1983). In addition, Lagace et al. (1983) and Putkey et al. (1983) inferred amino acid sequences for eel and chicken calmodulin from the nucleotide sequences of multiple, overlapping cDNAs. Other than a single amino acid substitution in eel calmodulin (Lagace et al., 1983), the amino acid sequences of all vertebrate calmodulins characterized to date appear to be identical. Among invertebrates, higher plants, and protozoa, there are several amino acid substitutions relative to the vertebrate protein (Burgess et al., 1983; Van Eldik et al., 1982).

The calmodulin molecule contains four structural domains that are homologous to each other and to the four domains of troponin C (Watterson et al., 1980a). These structural domains contain regions homologous to the portions of parvalbumin that form a calcium binding structure (Kretsinger, 1980). The first and second domains of calmodulin are more closely related respectively to domains 3 and 4 than are other pairs of domains (Watterson et al., 1980a). This intramolecular sequence homology is the basis of hypotheses that calmodulin may have evolved by gene duplication of a one- or two-domain precursor (Vanaman et al., 1977; Erickson et al., 1980). Accordingly, calmodulin from phylogenetically earlier species such as *Tetrahymena pyriformis* and *Dictyostelium discoideum* might be more similar to the postulated precursors than calmodulin from phylogenetically later species. An inherent assumption of such phylogenetic analyses of structure and function is that regions of extended amino acid sequence identity among calmodulins from closely related and

† From the Laboratory of Cellular and Molecular Physiology, Howard Hughes Medical Institute and the Department of Pharmacology, Vanderbilt University School of Medicine, Nashville, Tennessee 37232 (D.R.M., D.M.R., and D.M.W.), and the Department of Molecular Biology, Albert Einstein College of Medicine, Bronx, New York 10461 (M.C.). *Received December 20, 1983.* This work was supported in part by grants from the National Institutes of Health (GM29723 and 5P01GM11301 to M.C. and GM30861 to D.M.W.) and the National Science Foundation (PCM 8242875 to D.M.W.).

0006-2960/84/0423-2891$01.50/0